

1 **A simulation of the large-scale drifting snow storm in a turbulent**
2 **boundary layer**

3 **Zhengshi Wang^{1,2}, Shuming Jia^{1,2*}**

4 ¹ State Key Laboratory of Aerodynamics, China Aerodynamic Research and
5 Development Center, Mianyang Sichuan 621000, China

6 ² Computational Aerodynamics Institute, China Aerodynamics Research and
7 Development Center, Mianyang, Sichuan 621000, China

8 * **Corresponding:** Shuming Jia (jjashm17@cardc.cn)

9 **Abstract.** Drifting snow storm is an important aeolian process that reshapes alpine
10 glaciers and polar ice shelves, and it may also affect the climate system and
11 hydrological cycle since flying snow particles exchange considerable mass and energy
12 with air flow. Prior studies have rarely considered the full-scale drifting snow storm in
13 the turbulent boundary layer, thus, the transportation feature of snow flow higher in
14 the air and its contribution are largely unknown. In this study, a large eddy simulation
15 is combined with a subgrid scale velocity model to simulate the atmospheric turbulent
16 boundary layer, and a Lagrangian particle tracking method is adopted to track the
17 trajectories of snow particles. A drifting snow storm that is hundreds of meters in
18 depth and exhibits obvious spatial structures is produced. The snow transport flux
19 profile at high altitude, previously not observed, is quite different from that near the
20 surface, thus, the extrapolated transport flux profile may largely underestimate the
21 total transport flux. At the same time, the development of a drifting snow storm
22 involves three typical stages, the rapid growth, the gentle growth and the equilibrium
23 stages, in which the large-scale updrafts and subgrid scale fluctuating velocities
24 basically dominate the first and second stage, respectively. This research provides an
25 effective way to get an insight into natural drifting snow storms.

26 **1 Introduction**

27 Snow, one type of solid precipitation, is an important source of material to mountain
28 glaciers and polar ice sheets, which are widespread throughout high and cold regions
29 (Chang et al., 2016; Gordon and Taylor, 2009; Lehning et al., 2008). A common
30 natural phenomenon over snow cover is the drifting snow storm, which occurs when
31 the wind speed exceeds a critical value (Doorschot et al., 2004; Li and Pomeroy, 1997;
32 Sturm and Stuefer, 2013). Drifting snow can entrain loose snow particles on the bed
33 into the air, which may be further transported to high altitude by turbulent eddies
34 (King, 1990; Mann et al., 2000; Nemoto and Nishimura, 2004). Drifting snow clouds
35 typically can range in thickness from tens to thousands of meters (Mahesh et al., 2003;
36 Palm et al., 2011), which may not only affect people's daily life by reducing the
37 visibility and producing local accumulation (Gordon and Taylor, 2009; Mohamed et
38 al., 1998), but also can influence the global climate system evolution by changing the
39 mass and energy balance of ice shelves (Cess and Yagai, 1991; Hanesiak and Wang,
40 2005; Hinzman et al., 2005; Lenaerts and Broeke, 2012).

41 Several field experiments on drifting snow storm have been performed (Bintanja,
42 2001; Budd, 1966; Dingle and Radok, 1961; Doorschot et al., 2004; Gallée et al.,
43 2013; Gordon and Taylor, 2009; Guyomarch et al., 2014; Kobayashi, 1978; Mann et
44 al., 2000; K Nishimura and Nemoto, 2005; Kouichi Nishimura et al., 2015; J. W.
45 Pomeroy and Gray, 1990; Sbuhei, 1985; Schmidt, 1982; Sturm and Stuefer, 2013)
46 since the middle of the last century. However, the measurements are commonly
47 conducted near the surface, thus, the drifting snow features at high altitude are

48 unknown, and the impacts of these features are difficult to assess. A thorough
49 investigation documenting the evolution process and structure of a full-scale drifting
50 snow storm is essential to understand this natural phenomenon and assess its impacts.

51 Drifting snow models, on the other hand, offer a panoramic view of the evolution
52 process of drifting snow and thus have become one of the most useful research
53 approaches. Many continuum medium models of drifting snow (Bintanja, 2000; Déry
54 and Yau, 1999; Schneiderbauer and Prokop, 2011; Uematsu et al., 1991; Vionnet et al.,
55 2013) have advanced the knowledge of natural drifting snow to a great extent.
56 However, a particle-tracking drifting snow model is still needed since the particle
57 characteristics and its motion require further investigation. Although a series of
58 particle tracking models (Huang et al., 2016; Huang and Shi, 2017; Huang and Wang,
59 2015; 2016; Nemoto and Nishimura, 2004; Zhang and Huang, 2008; Zwaafink et al.,
60 2014) have been established, these models have generally focused on the grain-bed
61 interactions and particle motions near the surface. Thus, a drifting snow model aimed
62 at producing a large-scale drifting snow storm in a turbulent boundary layer deserves
63 further exploration.

64 In this study, a drifting snow model in the atmospheric boundary layer that focuses
65 on the full-scale drifting snow storm is established. The wind field is solved using a
66 large eddy simulation for the purpose of generating a turbulent atmospheric boundary
67 layer. A subgrid scale (SGS) velocity is also considered to include the diffusive effect
68 of small scale turbulence. Finally, particle motion is calculated using a Lagrangian
69 particle tracking method. The large-scale drifting snow storm is produced under the

70 actions of large-scale turbulent structures combined with a steady-state snow saltation
 71 boundary condition for particles, and its spatial structures and transport features are
 72 analyzed.

73 **2 Model and methods**

74 **2.1 Simulation of a turbulent atmospheric boundary layer**

75 The mesoscale atmosphere prediction pattern ARPS (Advanced Regional Prediction
 76 System, version 5.3.3) is adopted to simulate the turbulent atmospheric boundary
 77 layer, in which the filtered three-dimensional compressible non-hydrostatic
 78 Naiver-Stokes equation is solved (Xue et al., 2001):

$$79 \quad \frac{\partial \rho}{\partial t} + \frac{\partial}{\partial x_i} (\rho \tilde{u}_i) = 0 \quad (1)$$

$$80 \quad \frac{\partial \rho \tilde{u}_i}{\partial t} + \frac{\partial \rho u_i \tilde{u}_j}{\partial x_j} = -\frac{\partial \tilde{p}^*}{\partial x_i} + B \delta_{i3} - \frac{\partial \tau_{ij}}{\partial x_j} \quad (2)$$

81 where ‘ \sim ’ represents variables that are filtered and the filtering scale is
 82 $\tilde{\Delta} = (\Delta x_1 \Delta x_2 \Delta x_3)^{1/3}$, in which Δx_i is the grid spacing along streamwise ($i=1$),
 83 spanwise ($i=2$) and vertical direction ($i=3$), respectively.

84 $\rho = p(1 - q_v / (\varepsilon + q_v))(1 + q_v) / (R_d T)$ is the air density, in which p , q_v , R_d and T are
 85 the pressure, the specific humidity, the gas constant ($287.0 \text{ J kg}^{-1} \text{ K}^{-1}$) and
 86 temperature of the air, respectively, and $\varepsilon=0.622$ is a constant. u_i is the
 87 instantaneous wind speed component, and x_i is the position coordinate. t is time,
 88 δ_{ij} is the Kronecker delta, $B = -g \rho' / \rho$ is the buoyancy caused by the air density
 89 perturbation ρ' , and g is the acceleration due to gravity. $p^* = p' - \alpha \nabla \cdot (\rho \mathbf{u})$ contains
 90 the pressure perturbation term and damping term, where $\alpha = 0.5$ is the damping

91 coefficient and ∇ is the divergence. The subgrid stress τ_{ij} can be expressed as
 92 (Smagorinsky, 1963):

$$93 \quad \tau_{ij} = -2\nu_t \tilde{S}_{ij} = -2(C_s \tilde{\Delta})^2 |\tilde{S}| \tilde{S}_{ij} \quad (3)$$

94 where $\tilde{S}_{ij} = 0.5(\partial \tilde{u}_i / \partial x_j + \partial \tilde{u}_j / \partial x_i)$ is the strain rate tensor and $|\tilde{S}| = \sqrt{2\tilde{S}_{ij}\tilde{S}_{ij}}$, C_s
 95 is Smagorinsky coefficient that is determined locally by the dynamic Lagrangian
 96 model (Meneveau et al., 1996).

97 **2.2 Governing equation of particle motion**

98 The trajectory of each snow particle is calculated using a Lagrangian particle tracking
 99 method. Since a snow particle has is almost 10^3 times more dense than air, airborne
 100 particles are assumed to process only gravity and fluid drag forces, and the governing
 101 equations of particle motion can be expressed as (Dupont et al., 2013; Huang and
 102 Wang, 2016; Vinkovic et al., 2006):

$$103 \quad \frac{dx_{pi}}{dt} = u_{pi} \quad (4)$$

$$104 \quad \frac{du_{pi}}{dt} = m_p \frac{V_{ri}}{T_p} f(Re_p) + \delta_{i3} g \quad (5)$$

105 where x_{pi} and u_{pi} are the position coordinate and velocity of the snow particle,
 106 respectively. m_p is the mass of the solid particle, V_r is the relative speed between
 107 the snow particle and air, and $T_p = \rho_p d_p^2 / 18\rho\nu$ is the particle relaxation time, where
 108 ρ_p is the particle density (900 kgm^{-3}), d_p is the particle diameter and
 109 $\nu = 1.5 \times 10^{-5} \text{ m}^2 \text{ s}^{-1}$ is the kinematic viscosity of air. $f(Re_p)$ can be expressed as
 110 (Clift et al., 1978):

111
$$f(Re_p) = \begin{cases} 1 & (Re_p < 1) \\ 1 + 0.15 Re_p^{0.687} & (Re_p \geq 1) \end{cases} \quad (6)$$

112 where $Re_p = V_r d / \nu$ is the particle Reynolds number.

113 Considering the large grid spacing in simulating an atmospheric boundary layer
 114 (where the information about turbulent vortices smaller than the grid size is missing),
 115 the SGS velocity is also included and attached on the particle. Namely, the local
 116 relative is expressed as $V_{ri} = \tilde{u}_i(x_p) - u_{pi} + u'_i$, in which $\tilde{u}_i(\vec{x}_p)$ is the resolved
 117 large-scale wind speed at the particle's position and is determined by the resolved
 118 wind speeds of surrounding grid points through the linear interpolation algorithm. The
 119 SGS velocity can be calculated from the SGS stochastic model of Vinkovic et al.
 120 (2006):

121
$$du'_i = \left(-\frac{1}{T_L} + \frac{1}{2\tilde{k}} \frac{d\tilde{k}}{dt} \right) u'_i dt + \sqrt{\frac{4\tilde{k}}{3T_L}} d\eta_i(t) \quad (7)$$

122 where $T_L = 4\tilde{k} / (3C_0\tilde{\varepsilon})$ is the Lagrangian correlation time scale. Here, $C_0 = 2.1$ is
 123 the Lagrangian constant, $\tilde{\varepsilon} = C_\varepsilon \tilde{k}^{3/2} / \tilde{\Delta}$ is the subgrid turbulence dissipation rate,
 124 $C_\varepsilon = 0.41$ is a constant, and $d\eta_i$ is the increment of a vector-valued Wiener process
 125 with zero mean and variance dt . \tilde{k} is the subgrid turbulent kinetic energy and can
 126 be obtained from the transport equation (Deardorff, 1980):

127
$$\frac{\partial \tilde{k}}{\partial t} + \tilde{u}_j \frac{\partial \tilde{k}}{\partial x_j} = \frac{v_t}{3} \frac{g}{\theta_0} \frac{\partial \tilde{\theta}}{\partial x_3} + 2v_t \tilde{S}_{ij}^2 + 2 \frac{\partial}{\partial x_j} \left(v_t \frac{\partial \tilde{k}}{\partial x_j} \right) + \tilde{\varepsilon} \quad (8)$$

128 where θ is the potential temperature and θ_0 is the surface potential temperature.

129 2.3 Initial conditions of snow particles

130 To generate a large-scale drifting snow storm, a steady-state snow saltation condition
 131 is set as the bottom boundary condition for particles. During drifting snow events, the

132 sum of residual fluid shear stress τ_f and particle-borne shear stress τ_p should be
 133 equal to the total shear stress τ , thus, the particle-borne stress can be expressed as:

$$134 \quad \tau_p = \tau - \tau_f \quad (9)$$

135 Here, the residual fluid shear stress τ_f is set to be the threshold shear stress τ_{yf}
 136 of drifting snow, which can be read as (Clifton et al., 2006):

$$137 \quad \tau_{yf} = A^2 g \bar{d}_p (\rho_p - \rho) \quad (10)$$

138 in which $A = 0.2$ is a constant, and \bar{d}_p is the mean diameter of the snow particles.

139 At the same time, the particle-borne shear stress at the surface can be calculated
 140 from the particle trajectories as (Nemoto and Nishimura, 2004):

$$141 \quad \tau_p = \sum_{i=1}^{n_{\downarrow}} m_i u_{pi\downarrow} - \sum_{i=1}^{n_{\uparrow}} m_i u_{pi\uparrow} \quad (11)$$

142 where m_i is the mass of particle and $u_{pi\downarrow}$ and $u_{pi\uparrow}$ are the horizontal speeds of
 143 impact and lift-off particles, respectively. n_{\downarrow} and n_{\uparrow} are the particle number per
 144 unit area in unit time of impact and lift-off grains, respectively, which should be
 145 equivalent in steady-state saltation. Thus, the number of lift-off particles per unit area
 146 is:

$$147 \quad n_{\uparrow} = n_{\downarrow} = \frac{\tau_p}{\langle m_i \rangle (1 - \langle e_h \rangle) \langle u_{pi\downarrow} \rangle} \quad (12)$$

148 in which $\langle \rangle$ indicates the overall average, and e_h is the horizontal restitution
 149 coefficient of snow particle. According to Sugiura and Maeno (2000), the mean
 150 horizontal restitution coefficient can be expressed as:

$$151 \quad \langle e_h \rangle = \begin{cases} 0.48 \theta_i^{0.01} & v_i \leq 1.27 \text{ms}^{-1} \\ 0.48 \left(\frac{v_i}{1.27} \right)^{-\log\left(\frac{v_i}{1.27}\right)} \theta_i^{0.01} & v_i > 1.27 \text{ms}^{-1} \end{cases} \quad (13)$$

152 where θ_i and v_i are the impact velocity and angle, respectively. Here, θ_i has a
 153 mean value of approximately 10° (Sugiura and Maeno, 2000), and $\langle v_i \rangle$ is set to be
 154 the threshold of impact velocity. Considering the steady-state saltation condition (one
 155 impact particle generates one ejecta on average), $\langle v_i \rangle$ is determined by setting
 156 ejection number $n_e = 0.51v_i^{0.6}\theta_i^{0.16}$ equal to 1. In this way, the mean horizontal
 157 velocity of impact particles can be obtained through $\langle u_{pi\downarrow} \rangle = \langle v_i \rangle \cos \langle \theta_i \rangle$.

158 Then, the velocities of lift-off particles can be obtained from the restitution
 159 coefficient of snow. The horizontal restitution coefficient obeys the normal
 160 distribution with a mean value given in Eq. 13, and a standard variance as follow
 161 (Sugiura and Maeno, 2000):

$$162 \quad \sigma^2 = \begin{cases} 0.07\theta_i^{-0.06} & v_i \leq 0.52 \text{ ms}^{-1} \\ 0.07\left(\frac{v_i}{0.52}\right)^{-\log\left(\frac{v_i}{0.52}\right)}\theta_i^{-0.06} & v_i > 0.52 \text{ ms}^{-1} \end{cases} \quad (14)$$

163 On the other hand, the vertical restitution coefficient can be described by a two
 164 parameter gamma function (see Eq. 17), in which the parameter α and β can be
 165 expressed as (Sugiura and Maeno, 2000):

$$166 \quad \alpha = \begin{cases} 1.22\theta_i^{0.47} & v_i \geq 0.84 \text{ ms}^{-1} \\ 1.22\left(\frac{v_i}{0.84}\right)^{\log\left(\frac{v_i}{0.84}\right)}\theta_i^{0.47} & 0.84 < v_i \leq 1.23 \text{ ms}^{-1} \\ 1.22\left(\frac{v_i}{0.84}\right)^{\log\left(\frac{v_i}{0.84}\right)}\left(\frac{v_i}{1.23}\right)^{-2\log\left(\frac{v_i}{1.23}\right)}\theta_i^{0.47} & v_i \geq 1.23 \text{ ms}^{-1} \end{cases} \quad (15)$$

$$167 \quad \beta = \begin{cases} 12.85\theta_i^{-1.41} & v_i \geq 0.84 \text{ ms}^{-1} \\ 12.85\left(\frac{v_i}{0.84}\right)^{-\log\left(\frac{v_i}{0.84}\right)}\theta_i^{-1.41} & 0.84 < v_i \leq 1.23 \text{ ms}^{-1} \\ 12.85\left(\frac{v_i}{0.84}\right)^{-\log\left(\frac{v_i}{0.84}\right)}\left(\frac{v_i}{1.23}\right)^{\log\left(\frac{v_i}{1.23}\right)}\theta_i^{-1.41} & v_i \geq 1.23 \text{ ms}^{-1} \end{cases} \quad (16)$$

168 In this condition, if some of the snow particles within the saltation layer are
169 transported to higher in the air by turbulent vortexes (the saltation layer becomes
170 undersaturated), more particles will lift-off from the surface to replenish the saltation
171 layer until a saturated state is reached.

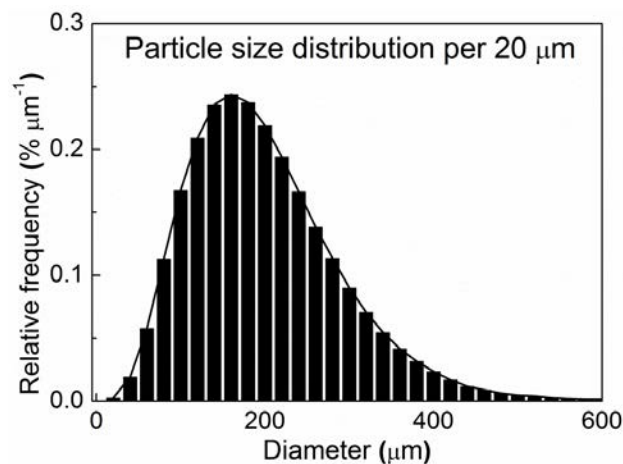
172 **2.4 Simulation details**

173 The computational domain is $1000\text{ m} \times 500\text{ m} \times 1000\text{ m}$, with a uniform horizontal
174 grid size of 5 m adopted to solve finer vortex structure in the atmospheric boundary
175 layer. The mean grid size in the vertical direction is 20 m, with a grid refinement
176 algorithm adopted near the surface (the finest grid size is 1 m). Periodic boundaries
177 are used along streamwise and spanwise dimensions, and the bottom is set as a grid
178 wall. The top is set as an open radiation boundary with a Rayleigh damping layer that
179 is 250 m in depth.

180 The atmosphere is neutral with an initial potential temperature of 300 K, and an
181 initial relative humidity of 90%. The initial wind profile is logarithmic with a surface
182 roughness of 0.1 m (Doorschot et al., 2004). Atmospheric turbulence is induced by
183 random initial potential temperature perturbations at the first-level grid level with a
184 maximum magnitude of 0.5 K, and is sustained by a constant heat flux at the bottom.
185 The constant heat flux is 50 Wm^{-2} according to the observation of Pomeroy and
186 Essery (1999). And the evolution time for a turbulent boundary layer is 5 times of the
187 large-eddy turnover time t_* ($\equiv H/u_*$, where H is the boundary layer depth and u_*
188 is the friction velocity). Actually, this condition corresponds to a ‘intermediate’
189 turbulent boundary layer that dominated by wind shear force (Moeng and Sullivan,

190 1994). Thus, the structures of the drifting snow storm should not be affected by the
191 changing surface heat flux significantly if the surface heat flux is small. Further
192 simulations with different values of surface heat flux ($<100 \text{ Wm}^{-2}$) also prove this
193 point.

194 For particles, periodic boundary conditions are also used at lateral boundaries, and
195 a rebound boundary condition without energy loss is adopted at the model top. The
196 bottom boundary condition for particles is given in Sect. 2.3, and is updated every 0.5
197 s. Additionally, each particle represents one particle parcel for the purpose of reducing
198 computational complexity. In this simulation, each particle parcel contains 10^7 snow
199 particles. The large time step and small time step (acoustic wave integral) for the wind
200 field calculation are 0.1 s and 0.02 s, respectively, and the particle time step is
201 determined by the minimum of particle relaxation time.



202
203 **Figure 1.** Size distribution of lift-off snow particles in this simulation.

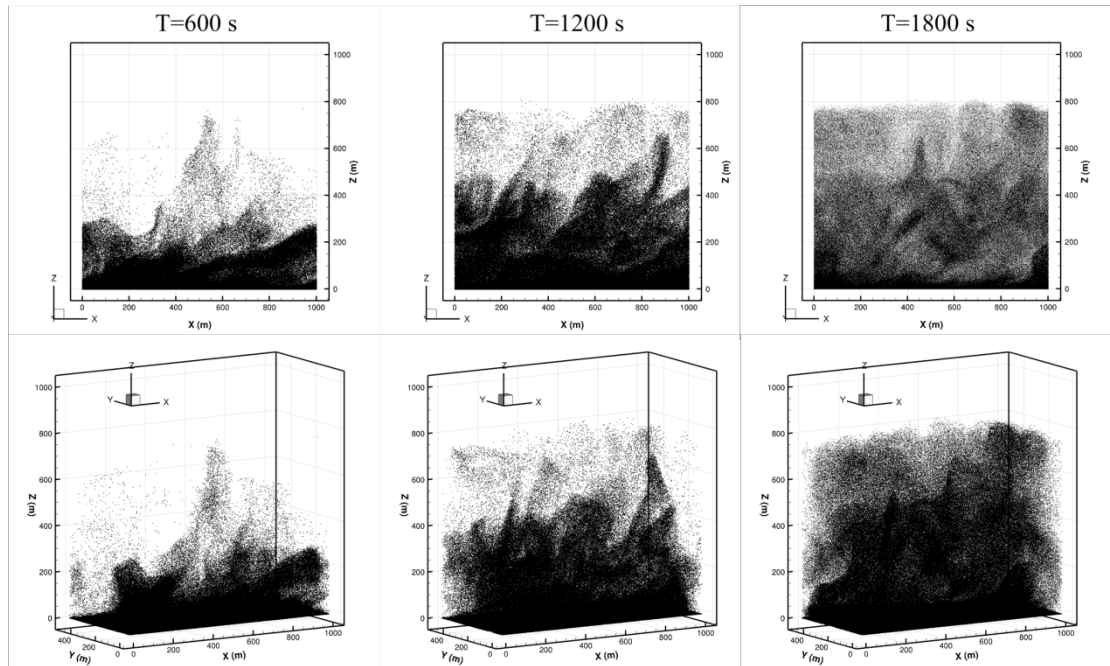
204 The size distribution of lift-off particles in drifting snow can be well described by
205 the two-parameter gamma function (Budd, 1966; Gordon and Taylor, 2009;
206 Nishimura and Nemoto, 2005; Schmidt, 1982):

207
$$f(d_p) = \frac{d_p^{\alpha_p - 1}}{\beta_p^{\alpha_p} \Gamma(\alpha_p)} \exp\left(-\frac{\beta_p}{d_p}\right) \quad (17)$$

208 where α_p and β_p are the shape and scale parameter of the distribution,
 209 respectively. In this simulation, the diameters of lift-off snow particles are given
 210 randomly from a gamma function with the parameters of $\alpha_p = 4$ and $\beta_p = 50$, as
 211 shown in Fig. 1, which is also consistent with observed particle size distributions
 212 (Nishimura and Nemoto, 2005; Schmidt, 1982).

213 3 Results and discussions

214 3.1 Model validation

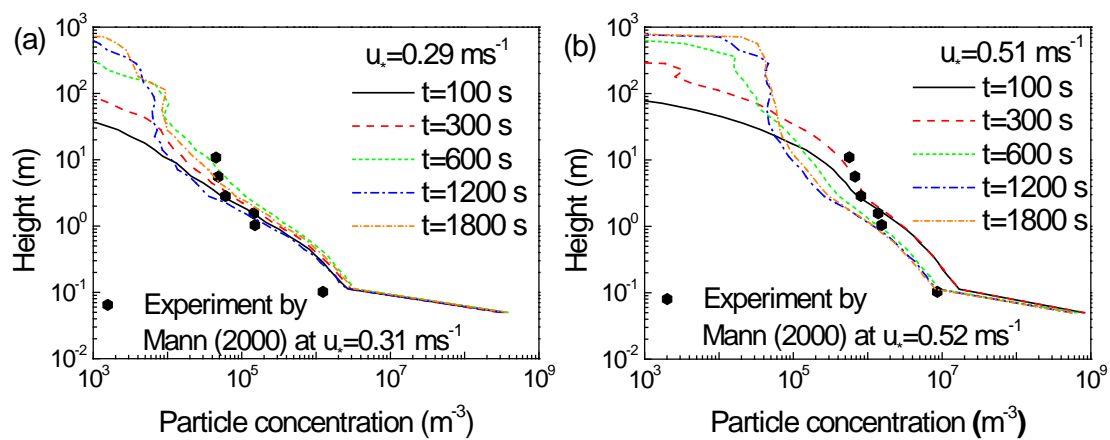


215 **Figure 2.** Drifting snow storm at different moments under the friction velocity of 0.29
 216 ms^{-1} .
 217

218 When drifting snow occurs in the atmospheric boundary layer, updrafts and
 219 turbulence fluctuations can send snow particles to high altitude, forming a fully
 220 developed drifting snow storm. Fig. 2 shows the drifting snow storm in the
 221 atmospheric boundary layer at different moments, in which the friction velocity is

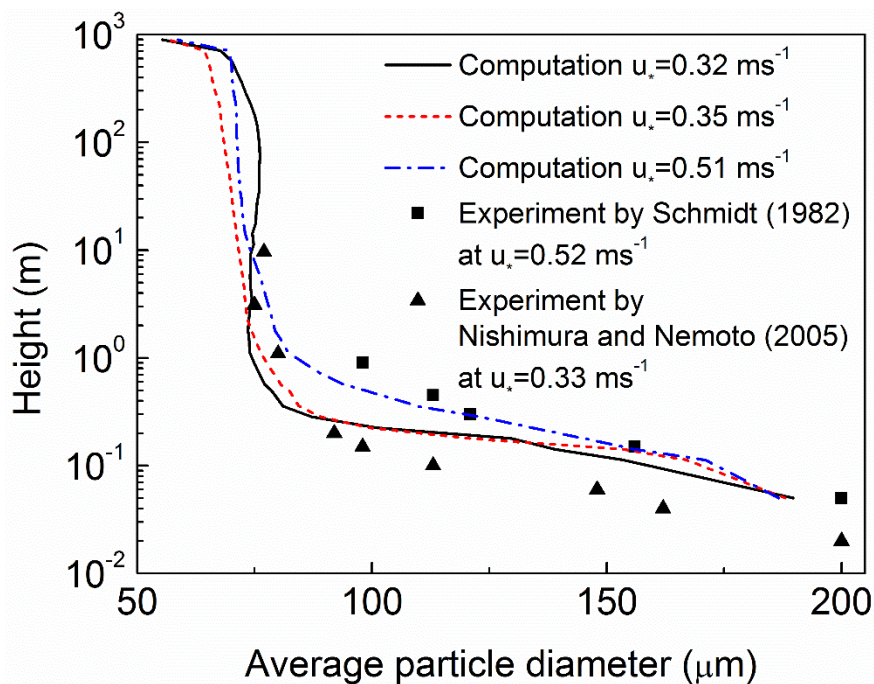
222 $u_* = 0.29 \text{ ms}^{-1}$ and dark spots represent snow particles. It can be seen that drifting
 223 snow storm experiences an evolution process from near the surface to high altitudes,
 224 which induces the fact that particle concentration decreases along increasing height.
 225 The high concentrations of drifting snow cloud are generally below 500 m, though
 226 snow particles may reach up to approximately 800 m under this condition. This is also
 227 consistent with observations (Mahesh et al., 2003; Palm et al., 2011).

228 Since a drifting snow storm exhibits a different structure from bottom to top, the
 229 evolution of particle number density profile in the drifting snow storm is shown in Fig.
 230 3, which is also compared with measurements of Mann et al. (2000). From this figure,
 231 the thickness of the drifting snow layer obviously increases with time, and almost
 232 approaches its steady state after 1200 s. At the same time, the particle number density
 233 basically decreases with height, which is consistent with the measurements of Mann
 234 et al. (2000) at various friction velocities. The predicted particle number density at the
 235 surface is much larger than at higher altitude and observations, mainly because the
 236 saltating particles are also included.



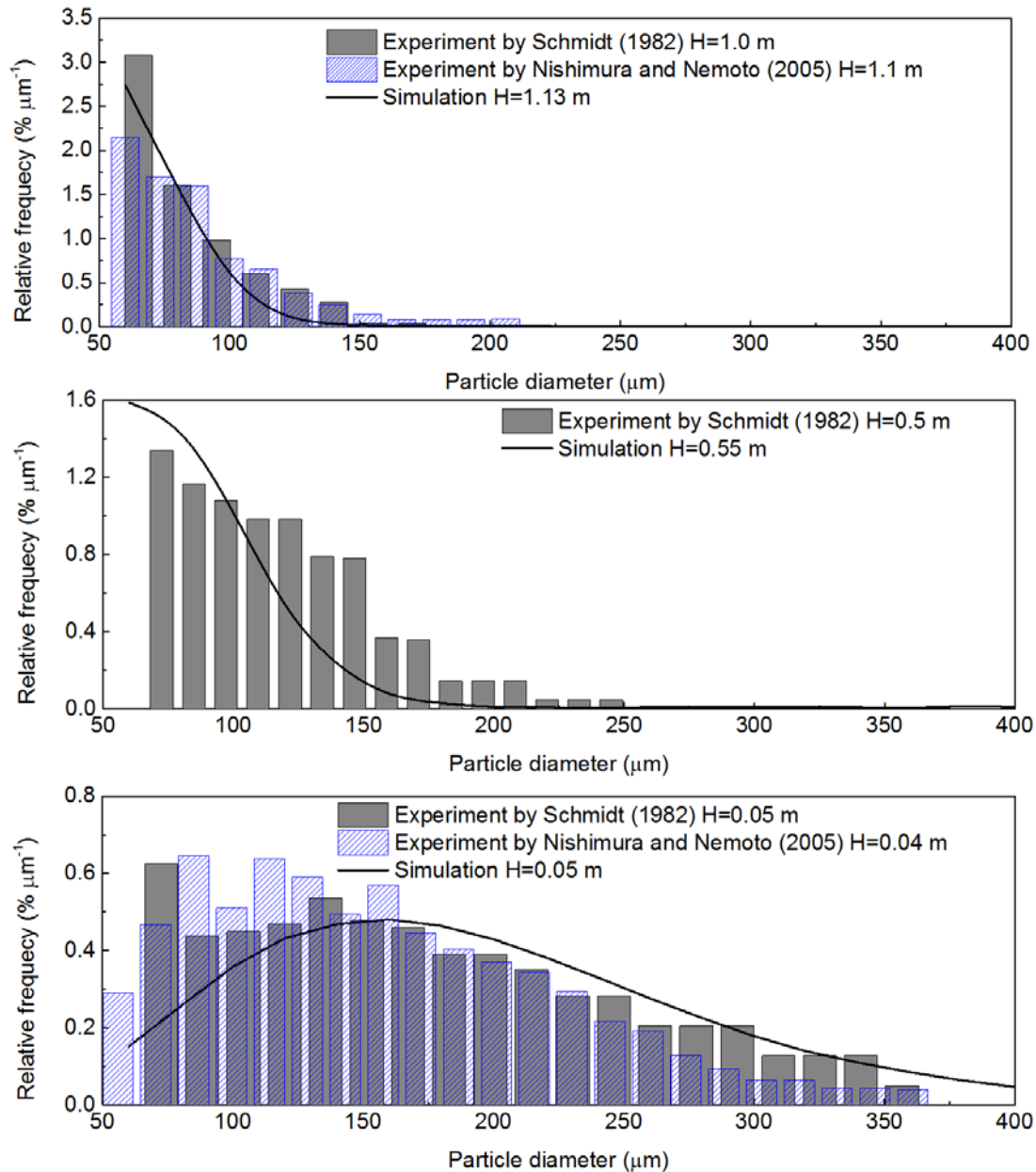
237
 238 **Figure 3.** Evolution of particle number density under various friction velocities (a)
 239 0.29 ms^{-1} and (b) 0.51 ms^{-1} .

240 Generally, smaller particles are more likely to be transported higher in the air. Fig.
 241 4 shows the variation of modeled average particle diameter versus height, which is
 242 also compared with various field measurements (Nishimura and Nemoto, 2005;
 243 Schmidt, 1982). Similar to the field observations, the average particle size basically
 244 decreases with height at lower altitude but is almost constant above 1 m. The average
 245 particle diameter is approximately 75 μm ranging from one meter to hundreds of
 246 meters in height, which is also consistent with the measurements of K Nishimura and
 247 Nemoto (2005).



248
 249 **Figure 4.** Variation of average particle diameter versus height.

250 Then, the particle size distributions at various heights are also compared with
 251 experiment results. As shown in Fig. 5, the heights are 0.05 m, 0.5 m and 1 m. The
 252 modeled particle size distributions at various heights are consistent with the
 253 measurements (Nishimura and Nemoto, 2005; Schmidt, 1982). Therefore, the
 254 established model is able to produce a large-scale drifting snow storm.



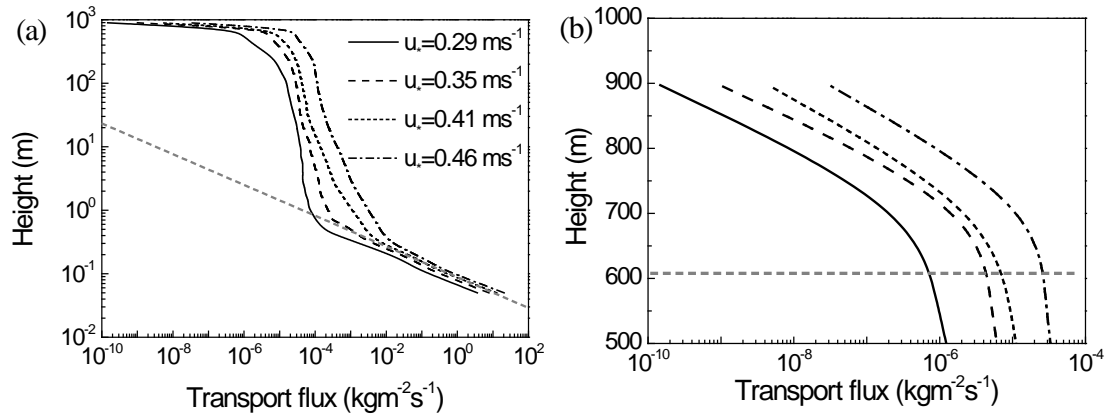
255

256 **Figure 5.** Particle size distribution at various heights.

257 Besides, it can be seen that the proportion of particles below 100 μm in diameter
 258 at 0.05 m is smaller than that of the experimental result. The reason could be that
 259 mid-air collisions, occurred frequently within the high concentration saltating snow
 260 cloud at the near surface, play an important role in conveying larger particles to
 261 higher altitude(Carneiro et al., 2013). However, the mid-air collision mechanism is
 262 beyond the scope of the current study.

263 **3.2 Snow transport flux**

264 The snow transport flux is of great importance to predict the mass and energy
265 balances of ice sheets. The total transport flux can be obtained from vertical
266 integration of the snow transport flux profile.



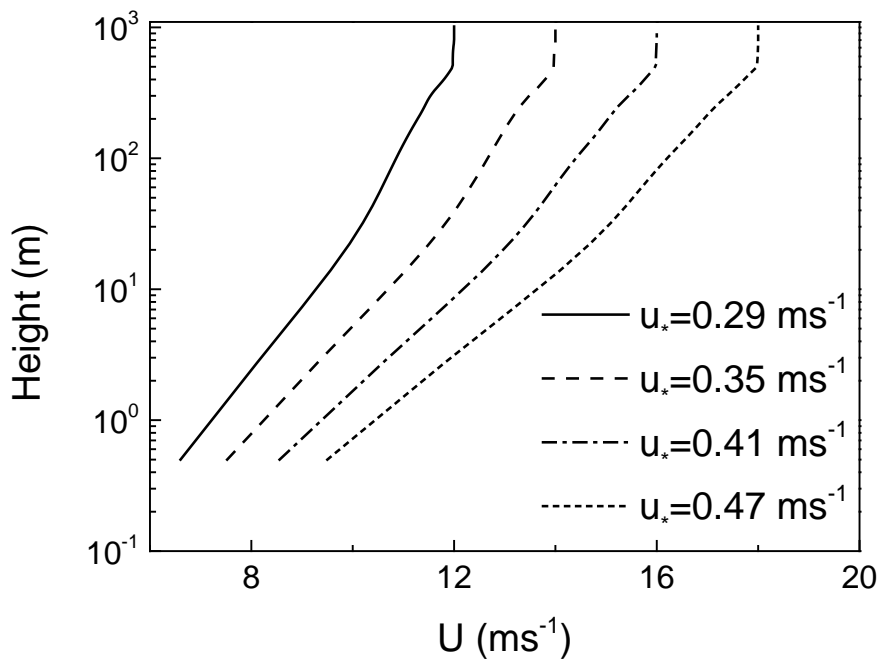
267

268 **Figure 6.** Variations of snow transport flux versus height.

269 The profiles of snow transport rate, per unit area, per unit time, under various
270 friction velocities are shown in Fig. 6(a). It can be seen that the transport flux
271 undergoes a sharp decrease with height at lower altitude (e.g., below 1.0 m), however,
272 the transport flux tends to decrease rather gentle until almost the top of the drifting
273 snow storm, as shown in Fig. 6(b), probably due to the large-scale turbulent motion
274 and increasing wind speed with height. In other words, the suspension flux of drifting
275 snow at higher altitudes, previously not observed, may be much larger than we
276 previously thought. The mean horizontal wind speed profiles of the fully developed
277 turbulent boundary layer under various friction velocities are shown in Fig. 7. The
278 horizontal wind speed increases with height and changes into a constant above the
279 boundary layer. The rapid decrease of the snow transport flux occurs at about the top
280 of the turbulent boundary layer, mainly because turbulences become weaker above

281 this height and less particles can be transported to a higher altitude.

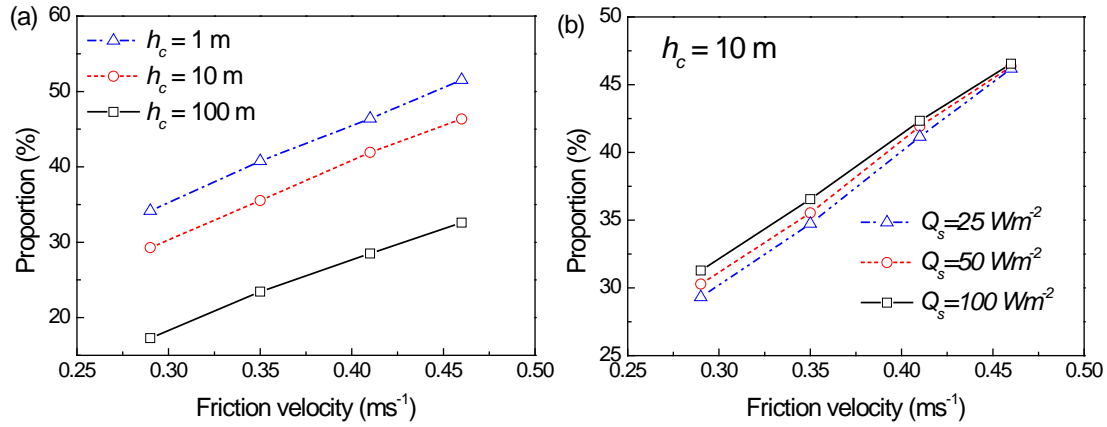
282 Besides, the transition of snow transport flux profile at about 1 m should be
283 mainly caused by the different motion states of particles with different particle sizes,
284 as shown in Fig. 4. Above the critical height, particles generally follow the turbulent
285 flow in the state of suspension because their gravities and relaxation times are small
286 enough. However, plenty of larger particles at the near surface make the particles
287 velocity differs from the wind speed, since particle inertia plays an important role.



288
289 **Figure 7.** Horizontal wind speed profiles of the fully developed turbulent boundary
290 layer under various friction velocities.

291 In previous studies, only the transport fluxes at the near surface are commonly
292 measured (Mann et al., 2000; Nishimura and Nemoto, 2005; Schmidt, 1982; 1984;
293 Tabler, 1991), thus, the features of the entire transport flux profile is largely unclear,
294 which may result in considerable uncertainties about the total transport flux. The
295 proportions of suspension flux above a given height h_c (referred as Q_c) to the total

296 suspension flux Q_s are shown in Fig. 7, in which snow particles below 0.1 m are not
 297 calculated (Mann et al., 2000).



298
 299 **Figure 8.** Proportion of suspension flux above h_c to the total suspension flux under
 300 (a) various friction velocities and (b) various surface heat fluxes Q_s .

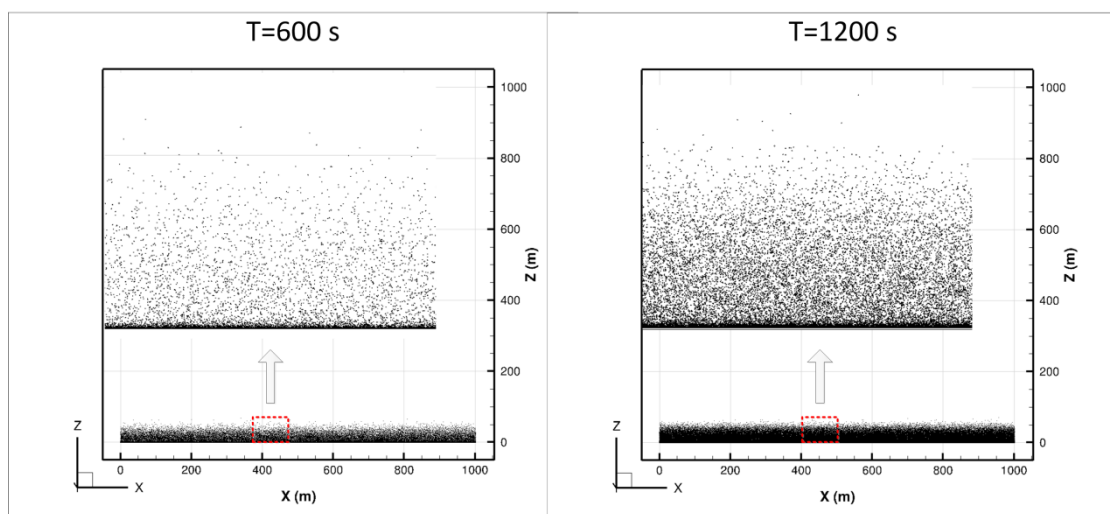
301 From Fig. 8(a), the contribution of Q_c to the total suspension flux is
 302 non-negligible under various h_c , the proportion of Q_c when $h_c = 100$ m to the total
 303 suspension flux has exceeded 30% when the friction velocity is 0.46 ms^{-1} . At the same
 304 time, the proportion of Q_c to the total suspension flux increases with friction
 305 velocity but decreases with increasing h_c . From Fig. 8(b), it can be seen that the
 306 proportion Q_c to the total suspension flux is only slightly affected by the surface
 307 heat flux, which indicates that the structures of drifting snow storm are not sensitive
 308 to the surface heat flux under this condition. The influence of surface heat flux is also
 309 weakened by the increasing friction velocity, mainly because larger friction velocity
 310 results in stronger turbulence under the actions of wind shear.

311 In this way, not only the snow transport flux, but also the sublimation of
 312 suspended snow particles should be reevaluated because the sublimation rate of snow
 313 particles higher in the air may be much larger than near the surface due to the lower

314 air humidity and greater wind speed at higher altitude (Mann et al., 2000; Nishimura
315 and Nemoto, 2005; Schmidt, 1982; 1984; Tabler, 1991).

316 3.3 Structures in a drifting snow storm

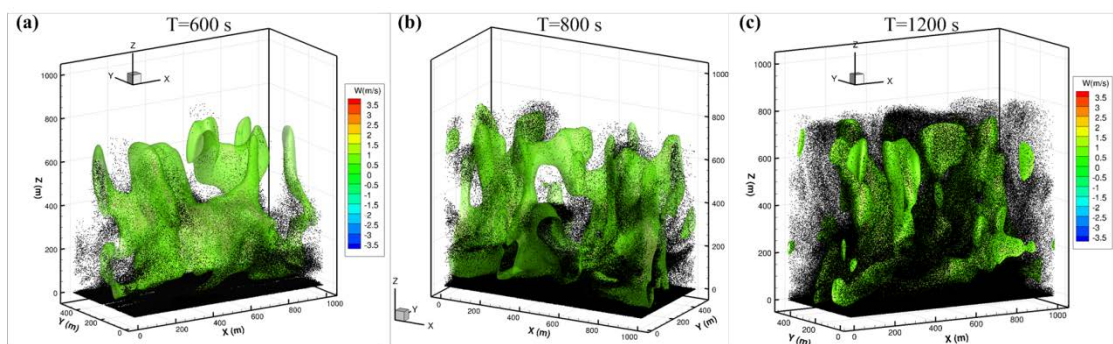
317 In a drifting snow storm, particles aggregate locally and produce special spatial
318 structures (as shown in Fig. 2). These structures should be directly related to the
319 turbulence structures present in the atmospheric boundary layer. Drifting snow storms
320 without atmospheric turbulence are shown in Fig. 9. This simulation is achieved by
321 replacing the resolved wind speed at particle's position ($\tilde{u}_i(\vec{x}_p)$) with a given value
322 obtained from the standard logarithmic profile, and the other model settings and
323 simulation procedures stay the same with other simulations. In this way, the effect of
324 large-scale turbulent structures on the development of the drifting snow storm
325 vanishes. Compared with Fig. 2, drifting snow particles mainly travel at the near
326 surface with a uniform spatial distribution when atmospheric turbulence is not
327 included.



328

329 **Figure 9.** Drifting snow storm without atmospheric turbulence under friction velocity
330 of 0.35 ms^{-1} .

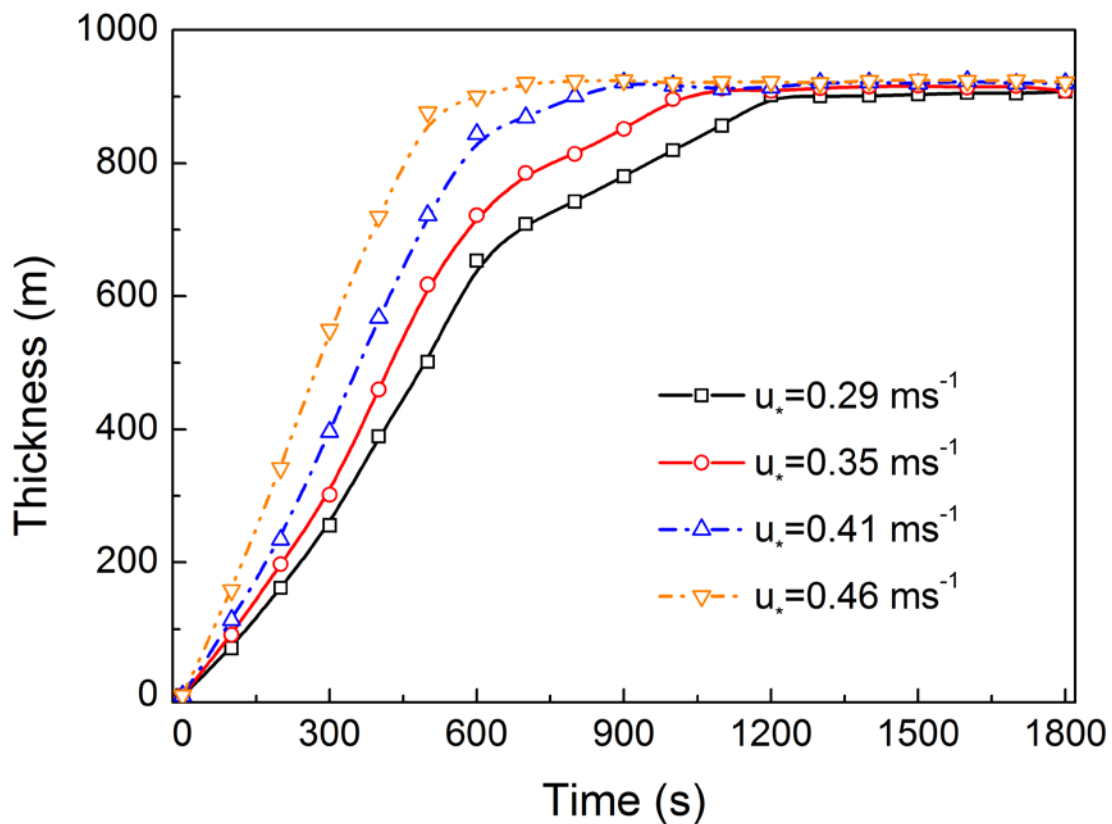
331 It is known that snow particles will become suspended if the local vertical wind
 332 speed exceeds the terminal velocity of particle. In a turbulent atmospheric boundary
 333 layer, there exists a large amount of turbulent structures with different scales and
 334 shapes. The vertical wind speed component of large-scale turbulence (namely, updraft)
 335 plays an important role in carrying snow particles to high altitude, while small scale
 336 turbulence (e.g., the SGS fluctuating velocity) tends to spread particles from high
 337 concentration zones to low concentration zones. As shown in Fig. 10(a), at the initial
 338 period of a drifting snow storm, the structures in the drifting snow storm are
 339 consistent with large-scale updrafts, and snow particles are mainly located in the
 340 updraft. With the further development of the drifting snow storm, as shown in Fig.
 341 10(b), more snow particles are scattered around the updraft bubbles although high
 342 concentration particle clouds are still in the wind bubbles. When drifting snow storm
 343 approaches its saturated state, snow particle clouds are almost connected together with
 344 numerous high concentration zones inside.



346 **Figure 10.** Evolution of drifting snow storm and vertical wind speed bubbles under
 347 friction velocity of 0.35 ms^{-1} , and wind bubbles are iso-surface of vertical wind speed
 348 with a value of 1.0 ms^{-1} (corresponding to the critical wind speed at which the particle
 349 of mean particle size becomes suspended particle, since the maximum diameter of

350 suspended particles is found to be approximately equals to the mean particle size of
351 the lift-off particles).

352 The evolution of the depth of drifting snow storm can be divided into three typical
353 stages. In sequence, these phases are the rapid growth phase, the gentle growth stage,
354 and an equilibrium state, as shown in Fig. 11. Here, the depth of drifting snow storm
355 refers to the average height of the topmost particle during this period (100 s). The
356 rapid growth stage is mainly driven by large-scale turbulent motion, while the
357 turbulent diffusion by the SGS fluctuating velocity is the main contributor to the
358 gentle growth stage. The duration of second stage decreases with increasing friction
359 velocity, which mainly comes from the stronger turbulent diffusion under larger
360 friction velocities.



361

362 **Figure 11.** Time evolutions of the thickness of drifting snow storm under various

363 friction velocities.

364 At the same time, the time required for the drifting snow storm to reach its
365 maximum thickness decreases with friction velocity, ranging from about 1200 s to
366 approximate 600 s when the friction velocity increases from 0.29 ms^{-1} to 0.46 ms^{-1} .
367 The thicknesses of saturated drifting snow storms are almost constant with a value
368 approximately 900 m under different friction velocities, probably because the
369 boundary layer depth as well as the surface heat flux are unchanged. Higher domain
370 heights are also tested with the same model settings, and the thickness of the drifting
371 snow seems basically unchanged. Drifting snow storm with difference thicknesses
372 may be achieved by changing the initial state of the air and surface heat flux. Thus,
373 the final thickness of a drifting snow storm should be largely dependent on the
374 maximum height of atmospheric turbulences.

375 **4 Conclusion**

376 In this work, large-scale drifting snow storms are simulated in a large eddy simulation
377 combined with a particle tracking model that includes subgrid scale velocity
378 fluctuations. A typical drifting snow storm of several hundred meters in depth is
379 generated, and the structure of the particle cloud with different concentrations is also
380 produced. The transport flux profile has obviously different slopes near the surface
381 compared to higher altitudes, that is, transport flux at near surface decreases with
382 height sharply, but decreases more gentle at higher altitude. Previous studies may
383 largely underestimate the total transport during drifting snow storms.

384 At the same time, the evolution of the thickness of drifting snow storm generally

385 contains three stages. Drifting snow storm development generally begins with a rapid
386 growth stage driven by the large scale atmospheric turbulent motions, followed by a
387 gentle growth stage driven by the SGS fluctuating wind speed, before reaching an
388 equilibrium stage when the drifting snow approaches a saturated state. The second
389 stage becomes shorter with increasing friction velocity, mainly because stronger
390 turbulence under higher friction velocity enhances the turbulent diffusion of particles.

391

392 *Acknowledgements.* This work is supported by the CARDC Fundamental and Frontier
393 Technology Research Fund (FFTRF-2017-08, FFTRF-2017-09), the National Natural
394 Science Foundation of China (11772143, 41371034), and National Key Research and
395 Development Program of China (2016YFC0500900).

396 **References:**

- 397 Bintanja, R.: Snowdrift suspension and atmospheric turbulence. Part I: Theoretical
398 background and model description, *Boundary-Layer Meteorology*, 95, 343-368,
399 2000.
- 400 Bintanja, R.: Characteristics of snowdrift over a bare ice surface in Antarctica, *Journal*
401 *of Geophysical Research Atmospheres*, 106, 9653-9659, 2001.
- 402 Budd, W. F.: The Byrd snow drift project : outline and basic results, American
403 Geophysical Union, Washington, DC, 71-134, 1966.
- 404 Carneiro, M. V., Araújo, N. A., Pähtz, T., and Herrmann, H. J.: Midair collisions
405 enhance saltation, *Phys.rev.lett*, 111, 058001, 2013.
- 406 Cess, R. D., and Yagai, I.: Interpretation of Snow-Climate Feedback as Produced by
407 17 General Circulation Models, *Science*, 253, 888-892, 1991.
- 408 Chang, A. T. C., Foster, J. L., and Hall, D. K.: Nimbus-7 SMMR Derived Global
409 Snow Cover Parameters, *Annals of Glaciology*, 9, 39-44, 2016.
- 410 Clift, R., Grace, J. R., and Weber, M. E.: Bubbles, drops, and particles, 263-264, 1978.
- 411 Clifton, A., Rüedi, J. D., and Lehning, M.: Snow saltation threshold measurements in
412 a drifting-snow wind tunnel, *Journal of Glaciology*, 52, 585-596, 2006.
- 413 Déry, S. J., and Yau, M. K.: A Bulk Blowing Snow Model, *Boundary-Layer*
414 *Meteorology*, 93, 237-251, 1999.
- 415 Deardorff, J. W.: Stratocumulus-capped mixed layers derived from a

416 three-dimensional model, *Boundary-Layer Meteorology*, 18, 495-527, 1980.

417 Dingle, W. R. J., and Radok, U.: Antarctic snow drift and mass transport, *Int. Assoc.*
418 *Sci. Hydrol. Publ.*, 55, 77-81, 1961.

419 Doorschot, J. J. J., Lehning, M., and Vrouwe, A.: Field measurements of snow-drift
420 threshold and mass fluxes, and related model simulations, *Boundary-Layer*
421 *Meteorology*, 113, 347-368, 2004.

422 Dupont, S., Bergametti, G., Marticorena, B., and Simoëns, S.: Modeling saltation
423 intermittency, *Journal of Geophysical Research Atmospheres*, 118, 7109-7128,
424 2013.

425 Gallée, H., Trouvilliez, A., Agosta, C., Genthon, C., Favier, V., and Naaim-Bouvet, F.:
426 Transport of Snow by the Wind: A Comparison Between Observations in Adélie
427 Land, Antarctica, and Simulations Made with the Regional Climate Model MAR,
428 *Boundary-Layer Meteorology*, 146, 133-147, 2013.

429 Gordon, M., and Taylor, P. A.: Measurements of blowing snow, Part I: Particle shape,
430 size distribution, velocity, and number flux at Churchill, Manitoba, Canada, *Cold*
431 *Regions Science & Technology*, 55, 63-74, 2009.

432 Guyomarch, G., Goetz, D., Vionnet, V., Naaimbouvet, F., and Deschatres, M.:
433 Observation of Blowing Snow Events and Associated Avalanche Occurrences,
434 *Preceedings, International Snow Science Workshop, Banff*, 2014.

435 Hanesiak, J. M., and Wang, X. L.: Adverse-Weather Trends in the Canadian Arctic,
436 *Journal of Climate*, 18, 3140-3156, 2005.

437 Hinzman, L. D., Bettez, N. D., Bolton, W. R., Chapin, F. S., Dyrgerov, M. B., Fastie,
438 C. L., Griffith, B., Hollister, R. D., Hope, A., and Huntington, H. P.: Evidence and
439 Implications of Recent Climate Change in Northern Alaska and Other Arctic
440 Regions, *Climatic Change*, 72, 251-298, 2005.

441 Huang, N., Dai, X., and Zhang, J.: The impacts of moisture transport on drifting snow
442 sublimation in the saltation layer, *Atmospheric Chemistry & Physics*, 16,
443 7523-7529, 2016.

444 Huang, N., and Shi, G.: The significance of vertical moisture diffusion on drifting
445 Snow sublimation near snow surface, *Cryosphere*, 11, 3011-3021, 2017.

446 Huang, N., and Wang, Z. S.: A 3-D simulation of drifting snow in the turbulent
447 boundary layer, *Cryosphere Discussions*, 9, 301-331, 2015.

448 Huang, N., and Wang, Z. S.: The formation of snow streamers in the turbulent
449 atmosphere boundary layer, *Aeolian Research*, 23, 1-10, 2016.

450 King, J. C.: Some measurements of turbulence over an antarctic ice shelf, *Quarterly*
451 *Journal of the Royal Meteorological Society*, 116, 379-400, 1990.

452 Kobayashi, S.: Snow Transport by Katabatic Winds in Mizuho Camp Area, East
453 Antarctica, *Journal of the Meteorological Society of Japan*, 56, 130-139, 1978.

454 Lehning, M., Löwe, H., Ryser, M., and Raderschall, N.: Inhomogeneous precipitation
455 distribution and snow transport in steep terrain, *Water Resources Research*, 44,
456 278-284, 2008.

457 Lenaerts, J. T. M., and Broeke, M. R. V. D.: Modeling drifting snow in Antarctica
458 with a regional climate model: 2. Results, *Journal of Geophysical Research*
459 *Atmospheres*, 117, D05109, 2012.

460 Li, L., and Pomeroy, J. W.: Estimates of Threshold Wind Speeds for Snow Transport
461 Using Meteorological Data, *Journal of Applied Meteorology*, 36, 205-213, 1997.

462 Mahesh, A., Eager, R., Campbell, J. R., and Spinhirne, J. D.: Observations of blowing
463 snow at the South Pole, *Journal of Geophysical Research Atmospheres*, 108, 4707,
464 2003.

465 Mann, G. W., Anderson, P. S., and Mobbs, S. D.: Profile measurements of blowing
466 snow at Halley, Antarctica, *Journal of Geophysical Research Atmospheres*, 105,
467 24491-24508, 2000.

468 Meneveau, C., Lund, T. S., and Cabot, W. H.: A Lagrangian dynamic subgrid-scale
469 model of turbulence, *Journal of Fluid Mechanics*, 319, 353-385, 1996.

470 Moeng, C. H., and Sullivan, P. P.: A Comparison of Shear- and Buoyancy-Driven
471 Planetary Boundary Layer Flows, *Journal of the Atmospheric Sciences*, 51,
472 999-1022, 1994.

473 Mohamed, N., Florence, N. B., and Hugo, M.: Numerical simulation of drifting snow:
474 erosion and deposition models, *Annals of Glaciology*, 26, 191-196, 1998.

475 Nemoto, M., and Nishimura, K.: Numerical simulation of snow saltation and
476 suspension in a turbulent boundary layer, *Journal of Geophysical Research*
477 *Atmospheres*, 109, D18206, 2004.

478 Nishimura, K., and Nemoto, M.: Blowing snow at Mizuho station, Antarctica,
479 *Philosophical Transactions*, 363, 1647-1662, 2005.

480 Nishimura, K., Yokoyama, C., Ito, Y., Nemoto, M., Naaim - Bouvet, F., Bellot, H.,
481 and Fujita, K.: Snow particle speeds in drifting snow, *Journal of Geophysical*
482 *Research Atmospheres*, 119, 9901-9913, 2015.

483 Palm, S. P., Yang, Y., Spinhirne, J. D., and Marshak, A.: Satellite remote sensing of
484 blowing snow properties over Antarctica, *Journal of Geophysical Research*
485 *Atmospheres*, 116, D16123, 2011.

486 Pomeroy, J. W., and Essery, R. L. H.: Turbulent fluxes during blowing snow: field
487 tests of model sublimation predictions, *Hydrological Processes*, 13, 2963-2975,
488 1999.

489 Pomeroy, J. W., and Gray, D. M.: Saltation of snow, *Water Resources Research*, 26,
490 1583-1594, 1990.

491 Sbuhei, T.: Characteristics of Drifting Snow at Mizuho Station, Antarctica, *Annals of*
492 *Glaciology*, 6, 71-75, 1985.

493 Schmidt, R. A.: Vertical profiles of wind speed, snow concentration, and humidity in
494 blowing snow, *Boundary-Layer Meteorology*, 23, 223-246, 1982.

495 Schmidt, R. A.: Transport rate of drifting snow and the mean wind speed profile,
496 *Boundary-Layer Meteorology*, 34, 213-241, 1984.

497 Schneiderbauer, S., and Prokop, A.: The atmospheric snow-transport model:
498 SnowDrift3D, *Journal of Glaciology*, 57, 526-542, 2011.

499 Smagorinsky, J.: General Circulation Experiments with the Primitive Equations,
500 *Monthly Weather Review*, 91, 99-164, 1963.

501 Sturm, M., and Stuefer, S.: Wind-blown flux rates derived from drifts at arctic snow
502 fences, *Journal of Glaciology*, 59, 21-34, 2013.

503 Sugiura, K., and Maeno, N.: Wind-Tunnel Measurements Of Restitution Coefficients

504 And Ejection Number Of Snow Particles In Drifting Snow: Determination Of
505 Splash Functions, *Boundary-Layer Meteorology*, 95, 123-143, 2000.

506 Tabler, R. D.: Snow transport as a function of wind speed and height, in: *Cold*
507 *Regions Engineering. Proceedings, Cold Regions Sixth International Specialty*
508 *Conference TCCP/ASCE, Cold Regions Engineering, 26-28 February 1991, West*
509 *Lebanon, NH, 729-738, 1991.*

510 Uematsu, T., Nakata, T., Takeuchi, K., Arisawa, Y., and Kaneda, Y.:
511 Three-dimensional numerical simulation of snowdrift, *Cold Reg.sci.technol*, 20,
512 65-73, 1991.

513 Vinkovic, I., Aguirre, C., Ayrault, M., and Simoëns, S.: Large-eddy Simulation of the
514 Dispersion of Solid Particles in a Turbulent Boundary Layer, *Boundary-Layer*
515 *Meteorology*, 121, 283-311, 2006.

516 Vionnet, V., Martin, E., Masson, V., Guyomarc'H, G., Naaimbouvet, F., Prokop, A.,
517 Durand, Y., and Lac, C.: Simulation of wind-induced snow transport in alpine
518 terrain using a fully coupled snowpack/atmosphere model, *Cryosphere Discussions*,
519 7, 2191-2245, 2013.

520 Xue, M., Droegemeier, K. K., Wong, V., Shapiro, A., Brewster, K., Carr, F., Weber, D.,
521 Liu, Y., and Wang, D.: The Advanced Regional Prediction System (ARPS) – A
522 multi-scale nonhydrostatic atmospheric simulation and prediction tool. Part II:
523 Model physics and applications, *Meteorology & Atmospheric Physics*, 76, 143-165,
524 2001.

525 Zhang, J., and Huang, N.: Simulation of Snow Drift and the Effects of Snow Particles
526 on Wind, *Modelling & Simulation in Engineering*, 2008, 408075, 2008.

527 Zwaafink, C. D. G., Diebold, M., Horender, S., Overney, J., Lieberherr, G., Parlange,
528 M. B., and Lehning, M.: Modelling Small-Scale Drifting Snow with a Lagrangian
529 Stochastic Model Based on Large-Eddy Simulations, *Boundary-Layer Meteorology*,
530 153, 117-139, 2014.